

Theory of luminescence polarization anisotropy in quantum wires

C. R. McIntyre and L. J. Sham

Department of Physics, University of California, San Diego, La Jolla, California 92093-0319

(Received 8 July 1991)

The polarization dependence of the optical transition is studied as a function of the aspect ratio of the rectangular cross section of a quantum wire. The effective-mass approximation is used to treat the valence- and conduction-band states. Calculated results lead to a simple physical understanding of luminescence polarization anisotropy.

I. INTRODUCTION

Quantum-well wires (QWW) have received intense research interest over the past few years because of the rich physical environment (i.e., reduced dimensionality, significance of interfacial roughness to transport, etc.) for the study of the confinement of electrons and holes. From a technological viewpoint, the optical characteristics of QWW are being investigated for applications to laser¹ and photodetectors.² In particular, the gain of QWW is theoretically³ predicted to be enhanced over that for quantum wells. The gain of QWW is proportional to the density of states for a two-dimensional system and the strength of the optical-matrix element. The density of states is enhanced for the first subband of the QWW over that of a quantum well.^{1,4} Optical experiments⁵⁻⁷ determining luminescence polarization dependence on the direction of the emitted light relative to the wire axis have been performed on QWW. These experiments have shown strong polarization anisotropy of the emitted light which is taken as a signature of confinement of carriers in the wire. Here, we focus on gaining a simple physical understanding of how confinement of valence holes in two dimensions leads to polarization anisotropy.

First, we present a theoretical model of a single QWW. In order to relate the results of our calculations to experiment, the effective-mass Hamiltonians and Bloch wave bases for the hole and electron are taken to be oriented along the axes of the quantum wire. The experimentally fabricated wires^{6,7} suggest a fairly realistic geometry for the wire if the wire is rectangular. Our study of the rectangular wire complements the studies of a wire of circular^{8,9} or square¹⁰ cross section. A way to understand the confinement effect of the wire is to vary the aspect ratio of the rectangular cross section from the quantum-well limit to a square.

In Sec. II, we give the details of the approximations for calculating the energies and wave functions of conduction electrons and valence holes confined to a wire of infinite length and rectangular cross section. In Sec. III, we present our calculation of the luminescence intensity as a function of the orientation of the polarization vector for three different aspect ratios of the rectangle. In Sec. IV, a discussion of the results is given.

II. THEORY

The following assumptions have been made to simplify the calculation.

(1) The wire is assumed to have a rectangular cross section and infinite length. QWW, formed by molecular-beam epitaxy (MBE) of GaAs/AlAs on vicinal substrates, have been fabricated in two types of deposition patterns, Tilted⁶ (TSL) and serpentine superlattices⁷ (SSL). Comparison of the energy levels for the rectangular cross section with the finite element analysis¹¹ of SSL's indicates that the confinement effect in the first few lowest levels of the conduction band is well described by the simple model. Therefore, the model can be used for photoluminescence (PL) which is dominated by the lowest-energy electron-hole recombination.

(2) The interior of the wire is assumed to be pure GaAs. Inadvertent mixture of the barrier material AlAs will be discussed in the last section.

(3) The barrier height is assumed to be infinite. The band offset for GaAs/AlAs is approximately 1.06 eV for the conduction band and 0.53 eV for the valence band.¹² We are interested only in the lowest conduction subband and the uppermost valence subband, which are of the order of 10 meV from the band edges.

(4) The Luttinger Hamiltonian¹³ is used for the Γ_8 valence bands. The spin-orbit split-off band Γ_7 is ignored. Recently, it has been shown that the split-off valence band does not, in a substantial way, affect the highest valence subband.¹⁴

(5) We calculate the PL intensity by transitions from the lowest conduction to the highest valence subband edge, i.e., we consider the case $K_z=0$, with no particle momentum along the wire axis. Since the exciton is made up of states in the neighborhood of the band edges, the polarization dependence should be very similar.

(6) Terms linear in wave vectors in the Luttinger Hamiltonian are neglected.

In addition to these assumptions, we align the wire in the experimental crystal orientation. For both TSL and SSL, the GaAs/AlAs lateral superlattices are deposited on tilted (from 0.5° to 4°) vicinal GaAs [100] substrates. The tilt is toward the $[0\bar{1}1]$ direction. These two axes form the plane of the cross section. The wire axis is

oriented along $[0\bar{1}\bar{1}]$. Given the orientation of the wires in the experiment, the Luttinger Hamiltonian is rotated so that the wave-vector component K_z is oriented parallel to the wire axis along $[0\bar{1}\bar{1}]$, K_x is parallel to the step direction $[0\bar{1}\bar{1}]$, and K_y is along $[100]$, the growth direction (Fig. 1). This yields

$$\underline{H}^{\text{rot}}(K_x, K_y, K_z) = \begin{pmatrix} P+Q & -S & R & 0 \\ -S^* & P-Q & 0 & R \\ R^* & 0 & P-Q & S \\ 0 & R^* & S^* & P+Q \end{pmatrix},$$

where

$$\begin{aligned} P &= \frac{-\gamma_1}{2} K^2, \\ Q &= - \left[\frac{3\gamma_3 - \gamma_2}{4} \right] K_x^2 - \frac{\gamma_2}{2} K_y^2 + \left[\frac{\gamma_2 + 3\gamma_3}{4} \right] K_z^2, \\ R &= \sqrt{3} \left[\left[\frac{\gamma_2 + \gamma_3}{4} \right] K_x^2 - \frac{\gamma_2}{2} K_y^2 - i\gamma_3 K_x K_y \right. \\ &\quad \left. + \left[\frac{\gamma_2 - \gamma_3}{4} \right] K_z^2 \right], \\ S &= -\sqrt{3}(\gamma_2 K_x - i\gamma_3 K_y) K_z. \end{aligned} \quad (1)$$

The notation used in Eq. (1) follows that of Ref. 13. Setting $K_z = 0$ and rearranging the Hamiltonian, we arrive at the block-diagonal form¹⁵

$$\underline{H}^{\text{rot}}(K_x, K_y, 0) = \begin{pmatrix} \underline{H}^U & 0 \\ 0 & \underline{H}^L \end{pmatrix}, \quad (2)$$

where

$$\begin{aligned} \underline{H}^U &= \begin{pmatrix} P+Q & R \\ R^* & P+Q \end{pmatrix}, \\ \underline{H}^L &= \begin{pmatrix} P-Q & R \\ R^* & P-Q \end{pmatrix}. \end{aligned}$$

Clearly, this Hamiltonian yields two sets of distinct eigen-

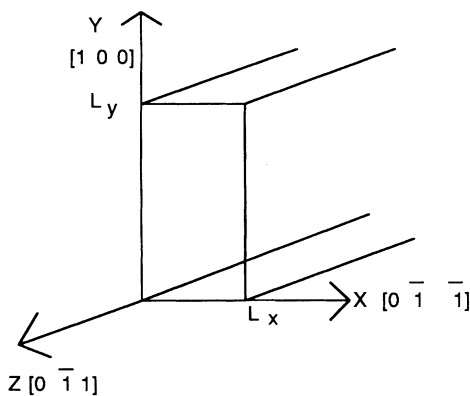


FIG. 1. Schematic of the quantum-well wire and its orientation to the $[100]$ substrate.

states which are doubly degenerate.

In the effective-mass approximation, the carrier wave function in the wire is the sum of products of the zone-center bulk Bloch wave function, U_j , and the associated envelope function which is slowly varying over the unit cell of the wire layer. The carrier wave function must satisfy the boundary conditions that $\Psi(x, y) = 0$ at the four interfaces of the wire. For the valence hole in the Luttinger representation, the basis set consists of the four Bloch waves at the top of the valence band, indicated by the index $j = \frac{3}{2}, \frac{1}{2}, -\frac{1}{2}, -\frac{3}{2}$. Each of the four-component envelope functions may be expanded as a double Fourier series¹⁶

$$\Psi_j^{(v)}(x, y) = \sum_{n_v, m_v} a_j(n_v, m_v) \sin(n_v K_x x) \sin(m_v K_y y), \quad (3)$$

where $K_x = \pi/L_x$, $K_y = \pi/L_y$, and L_x, L_y are the wire widths. The sine functions ensure the wave function vanishes at the boundary. The conduction electron wave function, with the spin state given by the index $s = \frac{1}{2}, -\frac{1}{2}$, is

$$\Psi_s^{(c)} = \frac{2}{\sqrt{L_x L_y}} \sin(n_c K_x x) \sin(m_c K_y y). \quad (4)$$

The eigenvalues and eigenvectors are computed including four terms in the series for the hole wave functions as a function of the aspect ratio (L_y/L_x), by diagonalizing the subblocks of Eq. (2). The uppermost valence-subband energy, which has a term proportional to $(L_y)^{-2}$ (the dimension of the wire) and is negative, becomes increasingly more negative as L_y decreases from infinity to L_x , which is kept fixed. These subbands and corresponding wave functions for different aspect ratios are used in determining the optical-matrix elements for different polarization directions.

III. LUMINESCENCE POLARIZATION

The optical-matrix element for transitions between conduction and valence bands is given by

$$|M|^2 = \sum_s \left| \sum_j \langle u_s | \mathbf{p} \cdot \mathbf{A} | u_j \rangle \langle \Psi_s^{(c)} | \Psi_j^{(v)} \rangle \right|^2, \quad (5)$$

where \mathbf{p} is the momentum operator and \mathbf{A} is the polarization vector of the emitted light. In the infinite-well approximation, from the overlap of the electron and hole envelope functions in Eq. (5), allowed transitions occur only between conduction- and valence-band states where $n_c = n_v$ and $m_c = m_v$. The results of the calculation are shown in Fig. 2. The three different curves represent aspect ratios equal to 1, 2, and 3. The optical strength for each aspect ratio is plotted as a function of the polarization direction varying from one coordinate axis to another. The graph indicates that maximum emission occurs for light polarized along the wire, the z axis.

For understanding the polarization anisotropy in a rectangular wire, we find it convenient, as we shall see in the next section, to express the wave function of the top

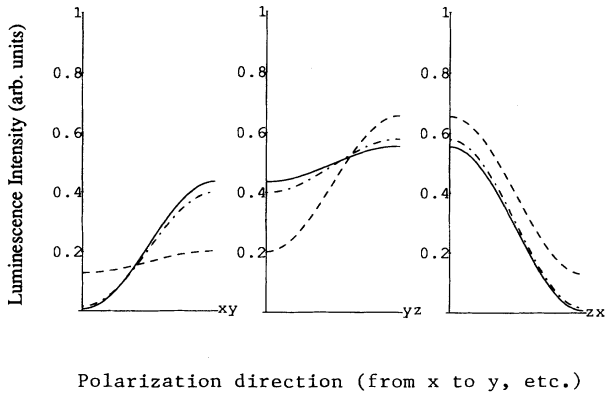


FIG. 2. Dependence of the luminescence intensity (in arbitrary units) on the angle of polarization varying from 0° to 90° from x to y , etc. Dashed, dash-dotted, and solid curves are for the aspect ratio = 1, 2, and 3, respectively.

valence subband state in terms of the p -like orbital basis¹⁷ of Bloch states $|X\rangle$, $|Y\rangle$, and $|Z\rangle$ times the spin-up or spin-down state instead of the spin- $\frac{3}{2}$ basis used above for the Luttinger Hamiltonian. For a cylindrical wire along the $[001]$ direction, the approximate cylindrical symmetry makes it convenient to consider the hole wave function in terms of the total angular momentum eigenstates.⁸ For the rectangular cross section, where total angular momentum about the wire axis is no longer a good quantum number, the basis states which reflect the symmetry of the rectangle are more appropriate. The modulus squared of the envelope functions as coefficients of $|X\rangle$, $|Y\rangle$, and $|Z\rangle$, for the three aspect ratios are plotted as functions of the coordinate x in the middle of the y dimension in Fig. 3.

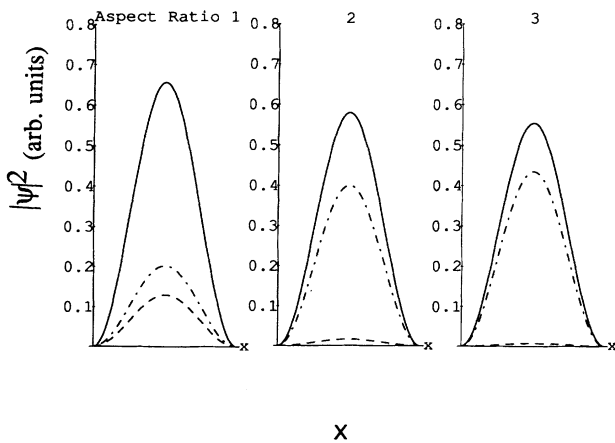


FIG. 3. Modulus squared of the envelope functions which are coefficients of the X , Y , and Z components of the valence bulk Bloch functions for the top valence subband state as a function of the coordinate x for a fixed y at $0.5 L_y$. Dashed, dash-dotted, and solid curves are associated with $|X\rangle$, $|Y\rangle$, and $|Z\rangle$, respectively.

IV. DISCUSSION

Experimental results from Ref. 7 indicate that the strongest emission occurs for light polarized parallel to the wire axis. Our theoretical results, shown in Fig. 2, show qualitatively the same behavior. The results can be explained in terms of the hole wave-function components $|X\rangle$, $|Y\rangle$, and $|Z\rangle$, shown in Fig. 3. These p -like orbitals are convenient because for the Bloch wave part of the transition matrix element in Eq. (5), $\langle u_s | p_\alpha | Z \rangle$ is finite only if $\alpha = z$.

Now keep L_x fixed and decrease L_y from infinity. For L_y at infinity, the system is a quantum well normal to the x direction. The top valence states are heavy-hole states with $j = \frac{3}{2}$, $-\frac{3}{2}$, with the spatial part $|Y \pm iZ\rangle$, i.e., equal amplitudes of $|Y\rangle$ and $|Z\rangle$. From the Bloch wave part of the transition-matrix element in Eq. (5), it follows that the light intensity is the same for the polarization vector along the y and z directions if the envelope functions are symmetric on interchanging y and z . They would be so if these were equivalent crystal directions. Actually, they are not quite equivalent so that there is a little anisotropy due to the difference between the $[100]$ and $[011]$ directions. The intensity decreases as the polarization changes its direction from y or z to x since the hole wave function contains no $|X\rangle$ component.

As the aspect ratio (L_y/L_x) decreases, confinement of the hole state along the y direction brings in a mixture of a small amount of the $|Z \pm iX\rangle$ state to $|Y \pm iZ\rangle$. This means the largest amount of $|Z\rangle$, a slightly small amount of $|Y\rangle$, and a small amount of $|X\rangle$. For the aspect ratio of 3, Fig. 3 confirms the relative amount of the three components. As the aspect ratio decreases, $|Z\rangle$ and $|X\rangle$ continue to grow and $|Y\rangle$ continues to wane until the amounts of $|X\rangle$ and $|Y\rangle$ become equal at the unit aspect ratio if the crystal anisotropy between x and y is neglected. The unequal amounts of $|X\rangle$ and $|Y\rangle$ in Fig. 3 are due to the crystal anisotropy between $[100]$ and $[011]$. The change in polarization anisotropy in Fig. 2 as the aspect ratio decreases simply reflects the change in the Cartesian components of the hole state. The overlap of the electron and hole envelope functions in Eq. (5) does not change much with the aspect ratio because the nodes are pinned at the boundaries.

While the above argument is based on the computation results of an infinite potential wall at the wire boundaries, the same reasoning for the polarization anisotropy may be used for the case of finite potential steps at the boundaries if the aspect ratio of the wire dimensions is changed to the effective aspect ratio of the wave function extents in the x and y directions. It is known from transmission electron microscope measurements on the tilted superlattice structure⁶ that Al and Ga intermix.¹⁸ It is believed also⁷ that there is intermixing of Al and Ga in the SSL's. To account for alloying of the wire and its environs, we expect the aspect ratio to be modified from the dimensions prescribed by the MBE deposition. Diffusion of Al in the step (x) direction lowers the potential barrier in the x direction and may produce an effective aspect ratio (L_y/L_x) lower than that of the as

grown geometrical dimensions. As is evident from Fig. 2, a lowering of the aspect ratio due to interdiffusion of Al and Ga will increase the luminescence intensity parallel to the wire direction. In SSL's, intermixing of Al and Ga in the barrier and well regions would increase the effective dimensions of the wire in both the x and y directions. The effective aspect ratio has to be computed from the two-dimensional highest hole state wave function.

ACKNOWLEDGMENTS

C.R.M. would like to acknowledge the Chancellor's Office of the University of California at San Diego for financial support. L.J.S. wishes to acknowledge the support from the NSF DMR 88-15068. We both thank the researchers and staff of the Center for Quantized Electronic Structures, University of California, Santa Barbara, where this work was done, for their hospitality.

-
- ¹Y. Arakawa and H. Sakaki, *Appl. Phys. Lett.* **40**, 939 (1982).
²D. L. Crawford, R. L. Nagarajan, and J. E. Bowers, *Appl. Phys. Lett.* **58**, 1629 (1991).
³M. Asada, Y. Miyamoto, and Y. Suematsu, *Jpn. J. Appl. Phys.* **24**, L95 (1985).
⁴H. Zarem, K. J. Vahala, and A. Yariv, *IEEE J. Quantum Electron.* **QE-25**, 705 (1989).
⁵J. Cibert, P. M. Petroff, G. J. Dolan, S. J. Pearton, A. C. Gosard, and J. H. English, *Appl. Phys. Lett.* **49**, 1275 (1986).
⁶M. Tsuchiya, J. M. Gaines, R. H. Yan, R. J. Simes, P. O. Holtz, L. A. Coldren, and P. M. Petroff, *Phys. Rev. Lett.* **62**, 466 (1989).
⁷H. Weman, M. S. Miller, H. Kroemer, P. M. Petroff, and J. L. Merz (unpublished).
⁸P. C. Sercel and K. J. Vahala, *Phys. Rev. B* **42**, 3690 (1990).
⁹P. C. Sercel and K. J. Vahala, *Appl. Phys. Lett.* **57**, 545 (1990).
¹⁰D. S. Citrin and Yia-Chung Chang, *Phys. Rev. B* **43**, 11 703 (1991).
¹¹M. S. Miller, C. E. Pryor, H. Weman, L. A. Samoska, H. Kroemer, and P. M. Petroff, in *Proceedings of the 20th International Conference on the Physics of Semiconductors*, edited by E. M. Anastassakis and J. D. Joannopoulos (World Scientific, Singapore, 1990), p. 1717; *J. Cryst. Growth* **111**, 323 (1991).
¹²G. Danan, B. Etienne, F. Molloy, R. Planel, A. M. Jean Louis, F. Alexandre, B. Jusseraud, G. Le Roux, J. Y. Marzin, J. Savary, and B. Sermage, *Phys. Rev. B* **35**, 6207 (1987).
¹³J. M. Luttinger, *Phys. Rev.* **102**, 1030 (1956).
¹⁴D. S. Citrin and Y.-C. Chang, *Phys. Rev. B* **40**, 5507 (1989).
¹⁵D. A. Broido and L. J. Sham, *Phys. Rev. B* **31**, 888 (1985).
¹⁶J. Xia and K. Huang, *Chin. Phys.* **8**, 1062 (1988); *Chin J. Semicond.* **8**, 568 (1987).
¹⁷E. O. Kane, *J. Phys. Chem. Solids* **1**, 249 (1957).
¹⁸J. M. Gaines, P. M. Petroff, H. Kroemer, R. J. Simes, R. S. Geels, and J. H. English, *J. Vac. Sci. Technol. B* **6**, 1378 (1988).